Ionospheric electron density over Resolute Bay according to E-CHAIM model and RISR radar measurements

Larson, B.; Koustov, A. V.; Themens, D. R.; Gillies, R. G.

DOI:
10.1016/j.asr.2023.01.017

Document Version
Publisher's PDF, also known as Version of record

Citation for published version (Harvard):
Larson, B, Koustov, AV, Themens, DR & Gillies, RG 2023, 'Ionospheric electron density over Resolute Bay according to E-CHAIM model and RISR radar measurements', *Advances in Space Research*, vol. 71, no. 6, pp. 2759-2769. https://doi.org/10.1016/j.asr.2023.01.017

Available online at www.sciencedirect.com

ScienceDirect

Advances in Space Research 71 (2023) 2759–2769

ADVANCES IN SPACE RESEARCH (a COSPAR publication)

www.elsevier.com/locate/asr

Ionospheric electron density over Resolute Bay according to E-CHAIM model and RISR radar measurements

B. Larson [a], A.V. Koustov [a,*], D.R. Themens [b,c], R.G. Gillies [d]

[a] Institute of Space and Atmospheric Studies, Department of Physics and Engineering Physics, University of Saskatchewan, Saskatoon, Saskatchewan, Canada

[b] Space Environment and Radio Engineering Group (SERENE), School of Engineering, University of Birmingham, Birmingham, UK

[c] Department of Physics, University of New Brunswick, Fredericton, New Brunswick, Canada

[d] Department of Physics and Astronomy, University of Calgary, Calgary, Alberta, Canada

Received 7 September 2022; received in revised form 5 January 2023; accepted 9 January 2023
Available online 13 January 2023

Abstract

In this study, predictions of the E-CHAIM ionospheric model are compared with measurements by the incoherent scatter radars RISR at Resolute Bay, Canada, in the northern polar cap. Reasonable coverage was available for all seasons except winter for which no conclusions were drawn. It is shown that ratios of the model-to measured electron densities are close to unity in the central part of the F layer, around its peak. This is particularly evident for summer daytime. Distributions of the ratios are wider for other seasons indicating larger number of cases when the model underestimates or overestimates. E-CHAIM underestimates the electron density at ionospheric topside and bottomside by ~ 10–20 %. At the bottomside, the underestimations are strongest in summer and equinoctial nighttime. At the topside, the underestimations are strongest in autumn nighttime. Model overestimations are noticeable in the middle part of the F layer during dawn hours in autumn. Overall, the model tends to not predict highest-observed peak electron densities and the largest-observed heights of the peak.

Keywords: E-CHAIM model; Incoherent scatter radars; Electron density; Polar cap; Modeling; Instruments and techniques; Ionospheric physics

1. Introduction

Knowledge of the electron density distribution in the Earth's ionosphere at extreme high latitudes is important for operation of radio communication systems and navigation (e.g., Belehaki et al., 2015; Rawer, 2013). Despite efforts (e.g., Kutiev et al., 2013), comprehensive characterization of the ionosphere as a function of external drivers of the near Earth's environment and reliable predictions of the ionospheric parameters at any instant of time is still far from being achieved. Part of the problem is a poor observational coverage in the High Arctic and Antarctic. It is not a surprise that a quick assessment of expected electron densities in these regions is often done by employing statistical ionospheric models such as International Reference Ionosphere (IRI) family of models (Bilitza et al., 2017; Bilitza, 2018). These models are mostly based on observations at the middle and auroral zone latitudes with very limited contributions from measurements in the polar cap regions.

Recently a new statistical model, the Empirical Canadian High Arctic Ionospheric Model (E-CHAIM), was proposed (Themens et al., 2017, 2018, 2019a). The model uses data from ground-based measurements at various lat-

* Corresponding author at: Institute of Space and Atmospheric Studies, University of Saskatchewan, Saskatoon, SK, Canada.
E-mail address: sasha.koustov@usask.ca (A.V. Koustov).

https://doi.org/10.1016/j.asr.2023.01.017
0273-1177/

itudes, and special efforts have been made to include polar cap ionosonde and radar observations in the Canadian sector of Arctic. E-CHAIM uses a semi-Epstein layer parameterization for its vertical structure, choosing to anchor the ionospheric electron density profile at the F2 peak and varying scale thickness with altitude to capture the features of the F1 and E regions (Themens et al., 2019a), as well as the behavior of electron density in the upper topside (Themens et al., 2018). The peak parameters of the model are represented by spherical cap harmonics in the Altitude Adjusted Corrected Geomagnetic Coordinates (AACGM) system (Shepherd, 2014). Separate fits of h_mF_2 and $\log 10(N_mF_2)$ were conducted for each UTC hour, resulting in 24 separate models for each parameter. The topside and bottomside thicknesses of the model are, however, represented by a single fit to harmonics in the AACGM MLT-MLat coordinate system. A further storm parameterization is also available for f_0F_2 to account for negative ionospheric responses to geomagnetic forcing (Maltseva and Nikitenko, 2021; Themens et al., 2017, 2020). Updates to the model since its initial public release in 2018 also include: 1) a parameterization of the auroral particle precipitation enhancement of the E region and lower F region (Watson et al., 2021) in E-CHAIM versions 2.0 and later, and 2) the inclusion of the Faraday IRI-2018 (FIRI-2018) model for specification at altitudes below the E region peak (Friedrich et al., 2018) in E-CHAIM versions 3.1 or later. Any of these additional features (storm, precipitation, D region) can be toggled on or off by the user but they are off by default. Complete details regarding any changes to the model since release can be found in the release notes provided with each version of the model. All versions of the model and their release notes have been preserved and are openly available on the E-CHAIM website (https://e-chaim.chain-project.net/). The model has been validated in a number of publications (Maltseva and Nikitenko, 2021; Shaikh, 2022; Themens et al., 2018, 2019a,b, 2021). It was shown that, generally, E-CHAIM improves quality of electron density predictions comparing to the IRI and NeQuick models but not in all aspects.

Recognizing the success of the E-CHAIM performance, first of all in terms of reproducing the solar cycle, seasonal and diurnal variations, there is still a great deal of uncertainty as to how good the model is for predictions of the electron density distribution in specific events. One area where these predictions would be useful is the Canadian Artic around Resolute Bay (RB), where three Super Dual Auroral Network (SuperDARN) high-frequency (HF) radars at Rankin Inlet, Clyde River and Inuvik are monitoring plasma flows (e.g., Nishitani et al., 2019). The geometry of these radars' observations is such that several their beams are close to the RB zenith. Knowing the electron density distribution in this area would allow for a better assessment of radar wave group ranges (mapping of a scattering volume) and derivation of the plasma drift from Doppler velocity measurements (Greenwald et al., 2016, 2017; Ponomarenko et al., 2009).

This study is aimed at further assessment of the E-CHAIM electron density predictions for the RB area. At RB, two incoherent scatter radars (ISR), RISR-North (RISR-N) and RISR-Canada (RISR-C) are operating, providing local and detailed information about the ionosphere. Reasonable agreement between ISR and E-CHAIM is expected, as the model used some RISR data during its development (Themens et al., 2017), and the bottomside predictions have been validated using an extended data base later (Themens et al., 2019a). The concern is that the ISR data contribution during the model development could have been overwhelmed by ionosonde data available for a much wider range of ionospheric conditions; furthermore, the ISR data were only used in the fitting of the E-CHAIM topside model and had no contribution to the bottomside, which relied entirely on ionosonde observations (Themens et al., 2018, 2019a). E-CHAIM is also an anchor point model and relies on independent sub-models for each component of its profile, so, while an evaluation of the independent components have been conducted in the respective model papers, the combined result of those models, i.e. for the entire electron density profile, has not been assessed, except via in situ measurements in the topside by Themens et al. (2019b, 2021). As success of the model is a culmination of the performance of each sub-model, it is critical that it be assessed as a whole. Furthermore, this is critical due to the potential for relatively small errors in individual model components combining to produce much larger (or potentially smaller) errors in electron density (Themens et al., 2021). More work comparing E-CHAIM and RISR radars could shed light on the reason for the discrepancies between the model and observations in specific events. Finally, new features are being added to the model and, consequentially, its periodical re-evaluation is required.

2. Instruments

This study uses ISR data (both RISR-N and RISR-C) collected in the World Day (WD) mode of operation with measurements in 11 beams (Bahcivan et al., 2010; Gillies et al., 2016) but only beams with elevation angles above 45° were considered here to restrict the considered area to the RB zenith. Long-pulse measurements with 5-min integration time were selected. RISR electron density profiles with shorter integration time are usually noisy, and, in addition, for a comparison with a statistical model, larger integration time (providing better signal-to-noise ratio) is preferable.

For the comparison undertaken, calibration of the electron density reported by the RISRs is a critical aspect of operation. The RISR radars routinely perform the calibration in one of the two ways: comparison with simultaneously received enhanced plasma line data or comparison with the co-located Canadian Advanced Digital Ionosonde (CADI) data. Calibrations with the CADI are performed by comparing the RISR-derived critical frequencies of the

F2 layer f_0F_2 and the height of the maximum h_mF_2 with those measured by the CADI. Values of f_0F_2 and h_mF_2 are obtained for the radars by fitting a 2-nd order polynomial to the electron density profile near the peak. To remove possible large differences between the radar and CADI due to differences in the sensing modality (e.g., CADI has a much larger field of view and thus much poorer spatial resolution), the comparison of f_0F_2 and h_mF_2 between the instruments is performed statistically, usually with several days of joint data. The median ratio of the f_0F_2 between the radar and CADI is used to derive a calibration constant for each radar beam. Finally, the fits of the ion-line data are reprocessed using the new calibration constants. The calibration procedure is repeated until the median ratio of ~ 1.0 is reached.

Fig. 1 gives a sense of a database available. Although all collected data were considered, the analysis was restricted to measurements between 100 and 500 km where the relative error was below < 50 %. Earlier data in 2014–2015 were collected by the RISR-N radar while after 2016, the database is strongly dominated by measurements with the RISR-C radar. We note that 50 % error restriction seems to be too relaxed, but not for the heights of $\sim$ 400–500 k m where strong variability is a persistent feature of RISR observations (Larson et al., 2021). Fig. 1 indicates that, seasonally, the autumn equinox has fewer points than the summer and spring equinox. The winter data are very limited. In terms of the time of day, the coverage seems to be better at daytime (the local noon at RB is close to 18 UT).

3. Average ionospheric electron density distribution over Resolute Bay

Despite the strong variability of the electron density distribution in the polar cap ionosphere, it is useful to know the average or typical electron density distribution over various seasons at certain locations. This allows one to, for example, predict the latitudes of echo bands in experimentation with HF radars, such as the SuperDARN radars (e.g., Nishitani et al., 2019), which is critical for the planning of future radar installations. In addition, knowledge of the background/average electron density values for a given location, season and time of day is necessary for the identification of polar cap patches and various space weather anomalies. For this reason, as a first step, typical electron density distributions over RB according to RISR measurements were inferred. Available data were sorted into seasons of three months each. The February, March and April data were grouped into spring. The summer season was represented by data from May, June and July. The September and October data were combined to represent autumn (no data were available for August). Finally, the data for January were considered as representing winter (no data were available for November and December).

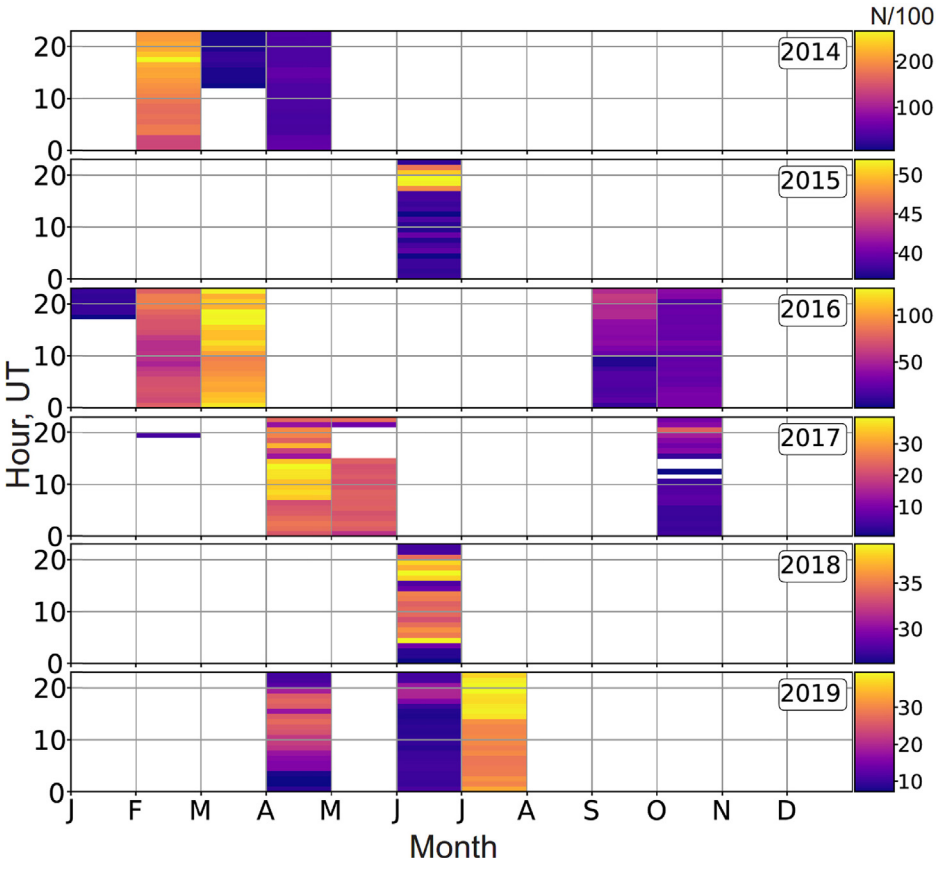

Fig. 1. Hourly number of points for RISR World Day mode experiments in the entire database considered in the study. The data were restricted to measurements at high elevation angle (>45°) beams and to those heights between 100 and 500 km at which the relative error was below 50 %.

Fig. 2 shows the median electron density for four seasons binned by altitude, using 25-km bins, and by one-hour bins of UT time. For RB, LT = UT-6 implying that the local noon is at 18 UT and the local midnight is at 6 UT. For the nighttime sector, that we loosely defined as the time between 03 and 09 UT, Fig. 2 shows that the electron density is somewhat larger in spring and summer as compared to autumn reaching peak values of $\sim 20 \times 10^{10}\, m^{-3}$ between 300 and 375 km in spring and 225 and 325 km in summer. Unfortunately, no data are available for the nighttime in winter.

The densities vary with time of day. For daytime, at 15–21 UT, the electron density is largest in spring with values up to $30 \times 10^{10}\, m^{-3}$ at heights of 250–450 km. Compared to spring, the electron densities are smaller in summer maximizing at the heights of 175–275 km, and they are even smaller in autumn. Winter data are limited; they indicate values comparable to those seen in autumn with a localized enhancement between 20 and 21 UT. For dusk, at 21–03 UT, the largest electron densities are in spring with values up to $\sim 30 \times 10^{10}\, m^{-3}$ at heights of 250–400 km. For dawn, at 9–15 UT, the electron densities are largest in summer with values up to $20 \times 10^{10}\, m^{-3}$ and lowest in autumn. The densities are maximized at largest heights in spring, at 250–350 km, and the electron density maxima are lowest in summer, at 200–300 km.

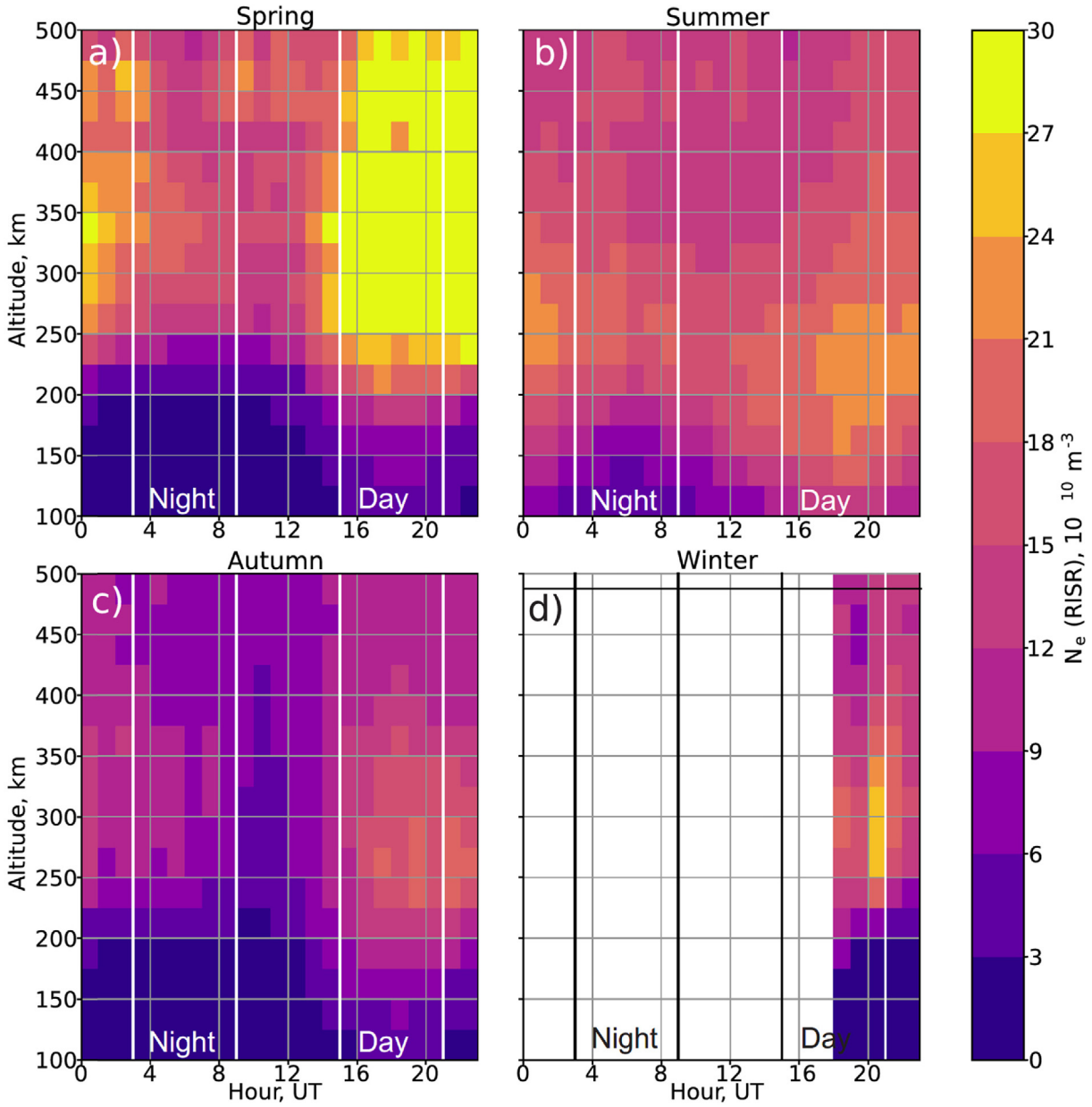

Fig. 2. Electron density distribution in the ionosphere over Resolute Bay according to RISR observations in 2014–2019. Presented are hourly median values over 25-km height bins.

One conclusion from the data of Fig. 2 is that, overall, peak electron densities occur at lower heights in summer (200–300 km) as compared to other seasons (300–400 km). For the equinoctial time, the electron densities are smaller in autumn as compared to spring at just about every height.

The RISR data in Fig. 2 show less pronounced diurnal variations of the topside electron densities compared to those at lower heights. For both spring and autumn, the largest electron densities are seen during daytime and dusk.

4. Comparison of E-CHAIM model output with ISR data

To compare E-CHAIM predictions with ISR data, the following approach was undertaken. For E-CHAIM, the C implementation of version 3.2.1 was used with the precipitation, storm and D region features on. E-CHAIM supports calculating N_mF_2 and h_mF_2 directly. The inputs for the model functions applied to other heights were time/-date, as well as altitude. For N_mF_2 andh_mF_2, a simple approach was taken with the exact RB location being adopted for calculations. When the same approach was implemented for comparison of the measured and predicted electron densities at various heights, it was found that there are significant differences in some local time sectors. As a result, a more sophisticated approach was adopted, with an E-CHAIM electron density prediction being generated for each RISR range gate in the dataset. In this approach, the model predictions were produced using the altitude, latitude and longitude for the center of each range gate.

4.1. Model-measurement comparison for the electron density peak

Fig. 3 compares E-CHAIM predictions and ISR measurements of N_mF_2 andh_mF_2. These two parameters are of interest to SuperDARN research (e.g., Koustov et al., 2020) but they are also focal parameters in empirical ionospheric models (e.g., Shubin, 2015; Themens et al., 2017). For Fig. 3, a limited RISR-C data set was used. The peak for RISR-C was identified by finding the maximum electron density value under 400 km along each radar beam and taking the median value for each set of high-elevation beams. The midpoint of the integration time of each scan was used when calculating N_mF_2 and h_mF_2 for E-CHAIM.

Fig. 3a shows N_mF_2 predicted by E-CHAIM versus N_mF_2 determined from RISR-C measurements as a scatter plot of the number of cases. Although there is significant point spread, the majority of the points are distributed close to the line of perfect agreement (bisector). The point distribution is asymmetric. It is stretched along the vertical (RISR) axis towards values $> 30 \times 10^{10}\, m^{-3}$ indicating that the model predicts very few cases with N_mF_2 values above$30 \times 10^{10}\, m^{-3}$.

Fig. 3b compares h_mF_2 between E-CHAIM and RISR-C. Similar to the comparison ofN_mF_2, the h_mF_2 pixel distribution is asymmetric with significant point stretching in the vertical direction toward higher RISR values. The model appears to have "an upper limit" of possible values as the model h_mF_2 are all below $\sim$ 320 km.

4.2. Model-measurement comparison at various heights

Now we compare E-CHAIM and ISR data at all heights where measurements were available. To make a quantitative judgment of the agreement, instead of presenting scatter plots, such as those in Fig. 3, we consider a ratio of E-CHAIM-modeled to RISR-measured electron density,$R_{E/R} = N_e^{ECHAIM}/N_e^{RISR}$. The inverse of this ratio has been considered by Bjoland et al. (2016) while assessing the IRI model with Svalbard ISR measurements.

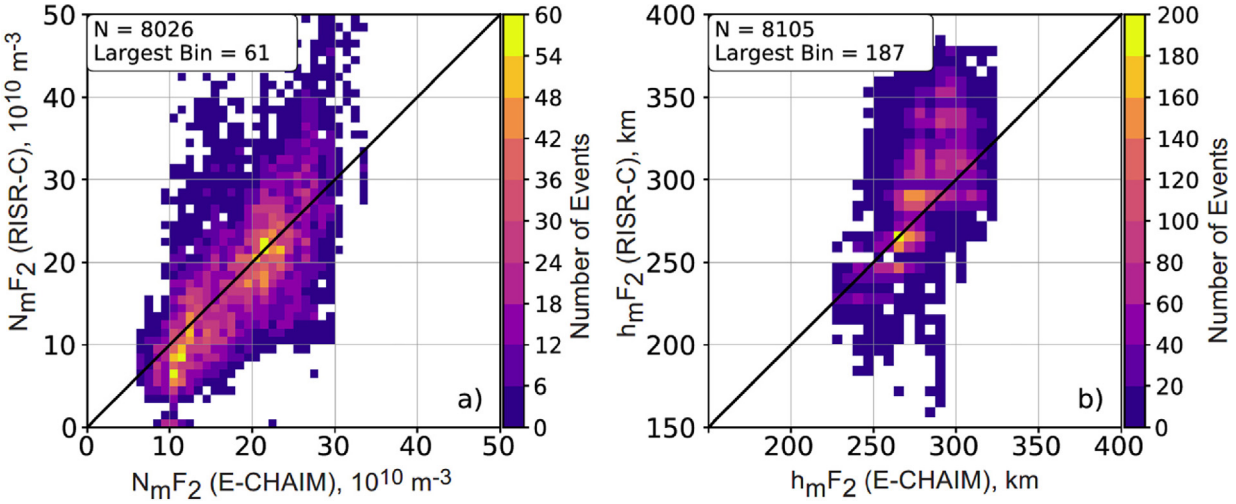

Fig. 3. (a) Scatter plot of the peak electron density N_mF_2 inferred from E-CHAIM versus RISR-based peak electron density N_mF_2 for matched moments. The total number of available points N is shown in the top left corner of each panel. The number of points in each pixel of the plot is coded according to the color bar to the right. (b) The same as (a) but for the height of the electron density peakh_mF_2.

Fig. 4 shows the UT distribution of $R_{E/R}$ at various heights for the four seasons selected. One overall conclusion from Fig. 4 is a fair consistency in the sense that, typically, $R_{E/R}$ values are in between 0.5 and 1.5 with very few "anomalies". The clear anomalies, with $R_{E/R}$ values up to 3, are for the heights of $\sim$ 150 km in the spring night sector (Fig. 4a) and in the winter afternoon/dusk sector (Fig. 4d). Data of Fig. 4b for summer show more uniform distribution over a day, compared to other seasons. $R_{E/R}$ values here are in between 0.9 and 1.2 in a wide range of heights, from $\sim$ 200 km to $\sim$ 400 km. Typical $R_{E/R}$ are smaller for both the bottomside and topside.

Data of Fig. 4a and 4c for equinoctial time show "islands" of increased $R_{E/R}$ above 1.5 in the autumn dawn sector (at 175 to 300 km) and especially in the spring nighttime sector (at 150–175 km). But the dominating color for the equinoctial time corresponds to $R_{E/R}$ values in between 0.9 and 1.2. For these seasons, similarly to summer, reduced $R_{E/R}$ values of $\sim$ 0.9 are seen at both the bottomside and topside. Limited winter data of Fig. 4d show that, apart from anomaly at 150–200 km, $R_{E/R}$ values are between 0.9 and 1.5 in the central part of the F layer while $R_{E/R}$ at the topside are typically $\sim$ 0.6.

Although Fig. 4 provides a good overview of the model-RISR differences, it contains many details that prohibit making conclusions on the overall quality of E-CHAIM predictions. For this reason, a more quantitative assessment was attempted by averaging ratios $R_{E/R}$ over time of

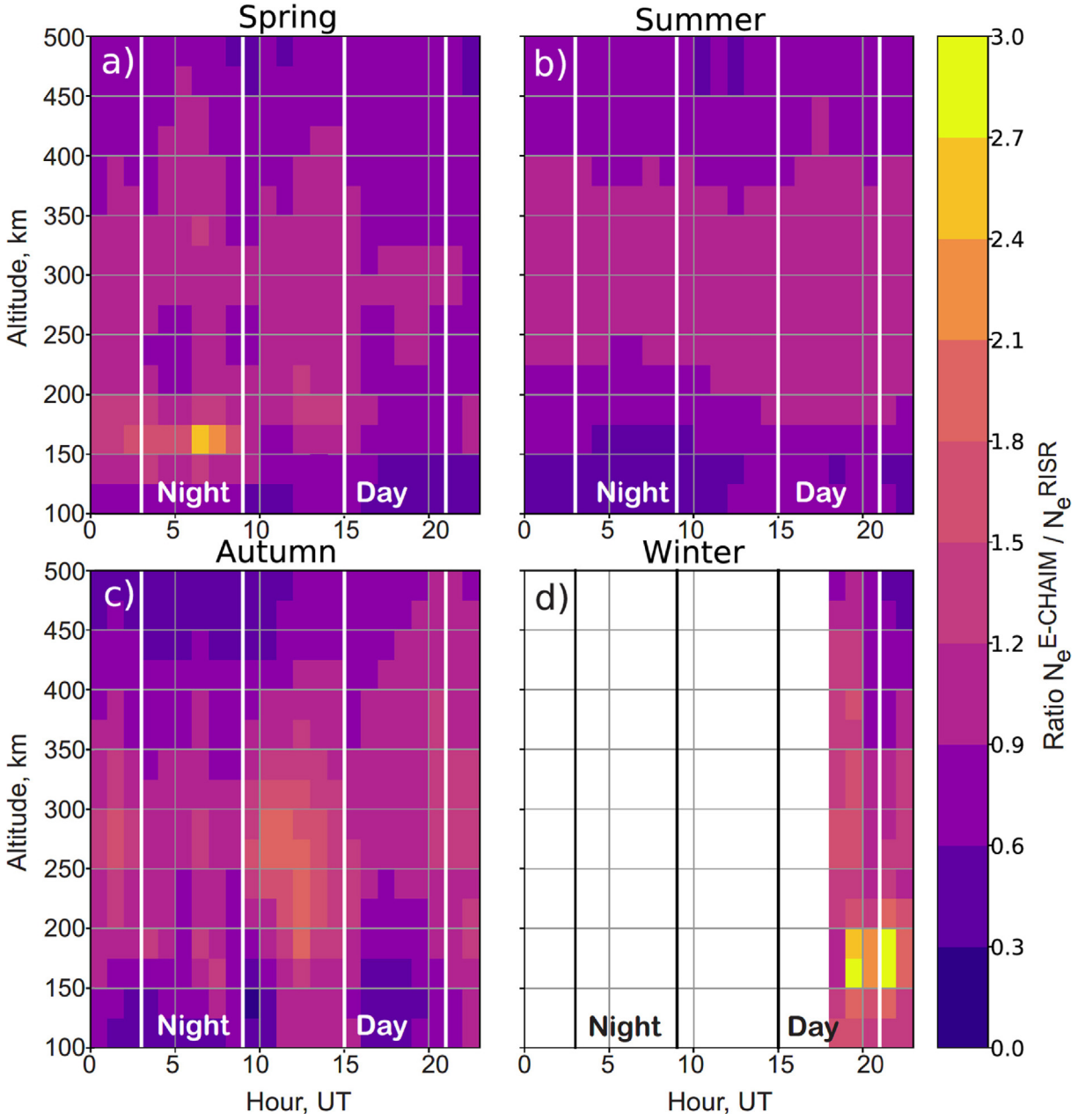

Fig. 4. The ratio of E-CHAIM-predicted to RISR-measured electron density for all events available in 2014–2019. The data have been grouped according to season, as indicated.

a day and over various heights. To this end, all available $R_{E/R}$ values were grouped by height region of the ionosphere: the bottomside spanning from 100 to 175 km, the middle F layer spanning from 175 to 425 km, and the topside covering 425–500 km altitudes. The histogram distributions of $R_{E/R}$ values were produced for each of these groups and for four seasons separately, Fig. 5. Each histogram was characterized by the median value μ and the standard deviation value σ. Obtained μ and σ values are reported on each plot. Since $R_{E/R}$ data were lumped into one set for each ionospheric part, the reported μ and σ values represent highly-averaged characteristics. Such an assessment sounds reasonable for summer conditions (Fig. 3) but, perhaps, somewhat over-simplification for other seasons with stronger diurnal variations. We should state that since the data set for winter is very limited, no conclusions will be drawn for this season. We also acknowledge that the number of autumn points is not as good as that for spring and summer, but still reasonably large.

Several general conclusions can be made from Fig. 5. All the distributions are asymmetric in shape with longer tails toward $R_{E/R}$ values of more than one reflecting cases of model overestimation. With very few exceptions, the overestimations are less than a factor of 2 in all heights, but more importantly, the bulk of the data are clustered around value of one. The distribution peaks are in between 0.5 and 1 indicating that overall, without looking into details, E-CHAIM tends to underestimate the electron density in the ionosphere over RB. The distribution width var-

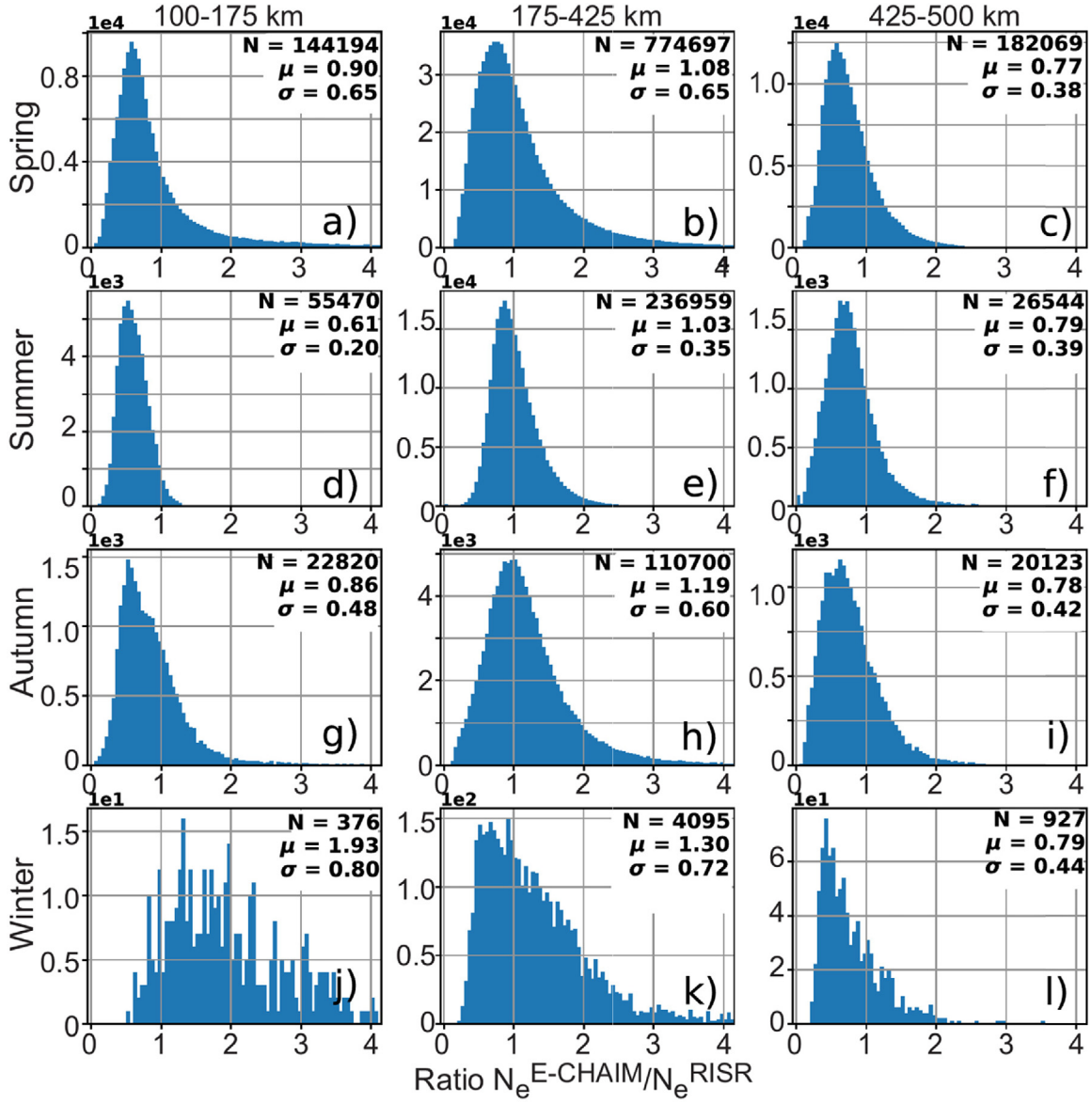

Fig. 5. Histogram distributions for the ratio of E-CHAIM-predicted to RISR-measured electron density at three different ranges of heights and for four seasons. Each histogram is characterized by the median value (μ) and the standard deviation value (σ), reported in the upper right corner. Also presented is the number of points N for each histogram.

ies with height and season. The distribution is narrowest in summer for every part of the ionosphere (Fig. 5d, 5e and 5f) and widest in spring at the bottomside and middle part of the F layer (Fig. 5a and 5b). Once again, we do not count the winter data with very broad distributions at the bottomside and near the F region peak (Fig. 5j and 5 k).

At the bottomside, the first column of plots in Fig. 5, the distribution medians are 0.90, 0.61 and 0.86, i.e. the model underestimates the electron density by 10–40 %. The model underestimations are strongest in summer. This contrasts with much better model-measurement agreement for other heights in summer. We note that the summer dataset for the bottomside is ~ 4 times smaller than that for the middle part of the F layer so that the strong bottomside model underestimation in summer needs to be re-evaluated in the future.

For the middle part of the F layer, middle column of plots in Fig. 5, $R_{E/R}$ values are much closer to 1, with medians μ being 1.08, 1.03 and 1.19. Summer data show the best data clustering (smallest values of σ) and μ closest to 1. Judging from the shape of the plots, the μ values away from 1 toward positive values are, to some extent, owing to the extended tails of large$R_{E/R}$. If largest $R_{E/R}$ values are not considered, μ values would be closer to 1. One must admit that the distribution peaks are somewhat shifted to values below 1 (with stronger effect in spring) offsetting the effect of large $R_{E/R}$ values. Overall, however, one can claim that the E-CHAIM model performs reasonably well in the middle part of the F layer.

For the topside ionosphere, right column of plots in Fig. 5, the distributions of $R_{E/R}$ are clearly centered at values below 1, both in terms of histogram medians (∼0.8) and positions of the distribution maxima (close to 0.7). These results imply that, here, the E-CHAIM model underestimates the electron densities by up to $\sim$ 20 %. Data spread seems to be smallest at these heights as σ values are smallest compared to those at other heights of the same season, except for the summer data. We note that the data coverage for the topside is $\sim$ 7 times better for spring (Fig. 5c) as compared to that for other seasons (Fig. 5f and 5i) implying that more data collection for those seasons is highly desirable.

5. Discussion

E-CHAIM performance has been assessed by the model developers in the past (Themens et al., 2017, 2018, 2019a,b, 2021) but the model is being updated so that further assessment work is warranted. The previous validation studies involved several instruments, including ISR data not utilized for the development of the model (Themens et al., 2018, 2019ab, 2021). More recent work by Themens et al. (2019a,b; 2021) has much more extensive coverage and included a significant amount of measurements from ISRs and onboard satellite sensors. For example, Themens et al. (2019b) utilized in situ data from Defense Meteorological Satellite Program (DMSP) satellites operating at $\sim$ 830 km and the Challenging Mini-satellite Payload (CHAMP) satellite operating between 350 and 400 km. The study compared E-CHAIM seasonal and solar cycle trends against measurements and showed a good agreement between DMSP and E-CHAIM with typical error of the order of$\sim 1 \times 10^{10}\, m^{-3}$. Thus E-CHAIM was validated in the topside ionosphere, well above the F region peak. At the typical altitudes of the F region peak, E-CHAIM was found to overestimate the electron density measured by CHAMP at latitudes $75^{\circ} - 85^{\circ}$ during summer daytime (Fig. 17) and winter nighttime but it correctly predicted the afternoon summer enhancement.

Themens et al. (2019a) focused on E-CHAIM performance at the ionospheric bottomside. The authors considered the extensive dataset collected by the Poker Flat ISR (covering 2007–2017) as well as data from RISR-N (2009–2017, but with better coverage for 2010–2013) and Svalbard (2007–2017) ISRs in the polar cap. The paper focused on bottomside with the thrust on the relative performance of the E-CHAIM and IRI models. Based on their Fig. 11, some conclusions with respect to the E-CHAIM model performance for individual events can be made. Fig. 11 shows that E-CHAIM underestimates electron density by $\sim$ 10 % at the ionospheric bottomside, 50–100 km below the height of the peak but overestimates by $\sim$ 10 % at lower heights, 150–200 km below the peak height. Underestimates are more evident in the winter midnight and dawn sectors while overestimates are more evident for summer daytime. Computed total electron content values for heights up to h_mF2 show domination of the underestimation effect all day long (Fig. 13).

The comparison undertaken in this paper differs from the previous work by Themens et al. (2019a) that was focused on the shape of the profile, not on the electron density as a whole. Here we compared the E-CHAIM climatological model with "instant" measurements at one specific point located deep in the polar cap. ISR data considered for this observational point constitute newer observations. In our study, the temporal resolution is shorter, 5 min instead of 15 min, and for the bins of the altitude we have taken the fixed value of 25 km versus varying bin sizes in Themens et al. (2019a). In addition, our data set is comprised of RISR-N and mostly RISR-C data in a long-pulse mode that hopefully provides robust determination of electron density at all heights considered.

The results of the present paper regarding N_mF_2 show comparable or somewhat less degree of consistency compared to the previous E-CHAIM validation work by Themens et al. (2017) who considered E-CHAIM predictions and ionosonde data, including the RB ionosonde. Themens et al. (2017) reported that modelled monthly-averaged plasma frequency f_0F_2 differs from ionosonde measurements by < 0.5 MHz. For a typical plasma fre-

quency of 5 MHz, an error in the model predictions would be 10 % for the plasma frequency and 20 % for the electron density. Scaling data for specific events from their Fig. 6 gives comparable values of model errors. Our comparison of modeled N_mF_2 and RISR values shows similar model-observation differences in the range of $N_mF_2 = (10 - 25) \times 10^{10}\, m^{-3}$ but the consistency deteriorates noticeably for larger values for which an error" in model predictions can be as large as $\sim$ 30 %, see data in Fig. 3a. For the heighth_mF_2, our Fig. 3b shows the model-measurement differences as large as 50–70 km at largest observed heights. This is well above the RMS model error of $\sim$ 13 km reported by Themens et al. (2017). Thus, our comparison indicates that large peak electron densities and large maximum heights are generally not predicted by E-CHAIM. In a way, this is consistent with Themens et al. (2020) who showed that E-CHAIM only captures $\sim$ 25 % of variability inN_mF_2. We attribute these findings to the fact that the model is a highly averaged representation of the real environment, and it cannot predict anomalously low and high values. In this view, further model-experiment comparisons at extreme conditions are of great interest, and this work is in our plans.

Our model-observation comparisons for various heights and seasons show a varying degree of consistency. Comparison for the middle part of the F layer showed model-to-measurement ratios $R_{E/R}$ close to 1, Fig. 4a, 4b, 4c and Fig. 5b, 5e, 5f, respectively. This is particularly evident in summer (Fig. 4b) for which the histogram distribution for ratio $R_{E/R}$ (Fig. 5e) is maximized near one. For other seasons (equinoctial time), the distributions are wider, the standard deviation of the distributions of 0.6–0.7 versus 0.36 for summer, indicating larger number of cases when E-CHAIM model overestimates or underestimates. The overestimations are prevailing in the autumn dawn sector (Fig. 4c) while the underestimations are recognizable in spring daytime (Fig. 4a). Because of these features, there is a shift of the distribution maxima towards a value smaller than one for spring (Fig. 4a) and towards unity for autumn (Fig. 4c). Better agreement for daytime and summer ionosphere is highly expected because the model itself was constructed using large amount of data from the RB ionosonde (data collected before 1995) with best coverage in these periods.

Qualitatively, having more events with model underestimations and overestimations in the middle of the F layer for seasons other than summer is consistent with the results by Themens et al. (2021) who considered total electron content (TEC) data from GPS receivers in the Canadian Arctic, including receivers at RB. According to their Fig. 8a, comparable values for the model and measurements are seen in summer with, perhaps, a minor underestimation. However, for autumn and spring, the minor model underestimations are recognizable at near noon and afternoon hours. We do expect a similarity in variations of TEC and F region electron density in its middle part because this part of the ionosphere contributes the most to TEC values.

Our analysis of E-CHAIM predictions for the bottomside ionosphere showed electron density underestimation for all seasons and most of the time, Figs. 4, 5a, 5d, 5 g (except of the localized in time anomaly for nighttime in spring, yellow spot in Fig. 4a). The medians of the distributions indicate a stronger underestimation effect in summer compared to equinoctial time, $R_{E/R}$~0.6 versus $\sim$ 0.9, but the distributions for $R_{E/R}$ are maximized at 0.7–0.8.

The E-CHAIM underestimation effect for the bottomside ionosphere is consistent with the results by Themens et al. (2019a) who compared E-CHAIM with data from the Poker Flat ISR in the auroral zone, e.g. their Figs. 9 and 15. Themens et al. (2019a) hinted that perhaps E-CHAIM has some biases on the bottomside because the model has been heavily reliant on ionosonde data. Ionosondes cannot detect low-density events so that the model should be biased toward larger electron density values. This effect, however, cannot not explain persistent model underestimation, but it can explain the anomalous overestimation for the spring nighttime, Fig. 4a. Indeed, Fig. 2a indicates that electron densities are very low during this period, compared to the summer case. However, following our explanation of the spring data, one would expect a similar "anomaly" of enhanced ratios for the autumn data. No obvious signatures of this expectation can be inferred from Fig. 4c. Another explanation is more realistic. Themens et al. (2019a) mentioned that enhanced auroral precipitation events can be responsible for model-measurement differences. Such precipitations can lead to noticeable model underestimation of the bottomside electron density, again because the model represents "averaged" conditions. All-in-all, our results indicate that bottomside E-CHAIM model needs further refinement.

In the topside ionosphere, the histogram distributions for $R_{E/R}$ were all shifted to values less than one (Fig. 5c, 5f, 5i) implying model underestimation. The medians of the distributions are close to 0.8 and the distribution peaks are also located at $\sim$ 0.8. Our conclusions for these heights are somewhat inconsistent with Themens et al. (2019b) who found good agreement between E-CHAIM and topside measurements, albeit at much larger heights (>830 km), their DMSP-IRI comparisons. At lower heights of $\sim$ 450 km, their comparison with Challenging Minisatellite Payload (CHAMP) data, their Fig. 17, clearly indicates that E-CHAIM overestimates during summer noon hours of low solar activity, between 2006 and 2009. We expect that the Langmuir Probe instrument on CHAMP underestimates the electron density, an effect well documented for the Swarm satellites (Larson et al., 20021; Lomidze et al., 2018). If this is indeed the case, then the data by Themens et al. (2021b) maybe be indicative of a minor model underestimation, consistent with our results.

One comment to add. Bjoland et al. (2016) compared predictions of the IRI model with Svalbard ISR measurements in the polar cap, similarly to what has been done

in our study for E-CHAIM and RISR. Some of their results are reminiscent of those reported here. For example (see their Fig. 5), their data also show best model-to-measurement ratios (closest to 1) in summer (note that Bjoland et al. (2016) presented results in terms of reverse ratios compared to ours). The IRI predictions were better for the heights around F region peak for all seasons with the worst agreement at dawn in autumn and winter. IRI also underestimates electron density at the bottomside and topside for all seasons although the ratios are much smaller, often reaching ~ 0.3, with more severe underestimations at the bottomside as compared to the topside.

6. Summary and conclusions

In this study, E-CHAIM model predictions of the electron density over Resolute Bay were compared with RISR incoherent scatter radar measurements. It was shown that the model-based peak electron density N_mF_2 is generally consistent with that reported by the RISR radar for the measured values in between$(10-25)\times 10^{10}\,m^{-3}$. For larger$N_mF_2$, the model underestimates. The model-based height of the electron density peak h_mF_2 is generally consistent with that measured by the RISR-C radar for the range of heights 220–300 km. The model shows smaller values for measured heights above 300 km. Thus, overall, the E-CHAIM model has a tendency not to show extreme N_mF_2 and h_mF_2 but predicts reasonably for the bulk of cases.

By splitting the database into three groups of heights, the bottomside, the middle part around the F region peak and the topside ionosphere, assessment of the model-observation consistency was performed for four seasons. Since data for winter were very limited, no conclusions were drawn for this season.

In terms of height, it was shown that E-CHAIM is in a reasonable agreement with measurements for the middle part of the F layer. Here the histogram distributions for the ratio of predicted-to-measured electron density are centered near 1 with the best coincidence in summer. At the topside altitudes, E-CHAIM underestimates electron densities with typical predicted-to-measured ratios of ~ 0.8. For the bottomside ionosphere, E-CHAIM underestimates electron densities as well, with typical predicted-to-observed electron density ratios being ~ 0.9 for equinoxes and ~ 0.6 for summer.

In terms of season, E-CHAIM performs somewhat better in summer with histogram distributions for the model-to-observation ratio being narrower and centered closer to 1, certainly for the middle part of the F layer. For other seasons (equinoctial time), the wider distributions indicate larger number of cases when E-CHAIM model overestimates or underestimates. In spring, the agreement is somewhat worse at noon-afternoon hours (18–24 UT). Moreover, strong overestimation was found for altitudes below 200 km at dawn. In autumn, the model-to-measured electron density ratios are somewhat better for the afternoon and dusk hours (18–24-02 UT) and the ratios are clearly above 1 at dawn (10–14 UT).

In terms of local time, model-to-measured electron density ratios vary with season and height. The daytime ratios are closest to unity at altitudes around the F layer peak in summer and worst at the bottomside in equinoxes. The nighttime ratios are better around the F layer peak in summer and worst at the bottomside in all seasons. The dusk ratios are comparable in a wide range of heights for all seasons with values less than one at the bottomside. The dawn ratios indicate strong overestimation in the middle part of the ionosphere in autumn and clear underestimation at the topside for all seasons.

Declaration of Competing Interest

The authors declare that they have no known competing financial interests or personal relationships that could have appeared to influence the work reported in this paper.

Acknowledgments

The research was supported by an NSERC Discovery grant and a research grant from CSA to A.V.K. The University of Calgary RISR-C radar is funded by the Canada Foundation for Innovation and is a partnership with the US National Science Foundation and SRI International. RISR-N operations were supported by NSF Cooperative Agreement 1840962 to SRI International.

E-CHAIM is supported under Defense Research and Development Canada contract number W7714-186507/001/SS and is maintained by the Canadian High Arctic Ionospheric Network (CHAIN) with operations support from the Canadian Space Agency. E-CHAIM version 3.2.1 was used in this work.

Statement on data availability

RISR-N/C data are available at the Madrigal database http://madrigal.phys.ucalgary.ca (both radars) or http://data.phys.ucalgary.ca (RISR-C). The data used in this work are also freely available through the NSF-supported Open Madrigal Initiative (http://cedar.openmadrigal.org/openmadrigal). The E-CHAIM model can be downloaded, after registration, from https://chain-new.chain-project.net/index.php/projects/chaim/e-chaim.

References

Bahcivan, H., Tsunoda, R., Nicolls, M., Heinselman, C., 2010. Initial ionospheric observations made by the new Resolute incoherent scatter radar and comparison to solar wind IMF. Geophys. Res. Lett. 37, L15103. https://doi.org/10.1029/2010GL043632.

Belehaki, A., Tsagouri, I., Kutiev, I., Marinov, P., Zolesi, B., Pietrella, M., Themelis, K., Alias, P., Tziotziou, K., 2015. The European ionosonde service: nowcasting and forecasting ionospheric conditions over Europe for the ESA Space simulational awareness services. J. Space

Weather and Space Climate 5, A25. https://doi.org/10.1051/swsc/2015026.

Bilitza, D., 2018. IRI the International Standard for the Ionosphere. Adv. Space Res. 16, 1–11. https://doi.org/10.5194/ars-16-1-2018.

Bilitza, D., Altadiil, D., Truhlik, V., Shubin, V.N., Galkin, I., Reinisch, B., Huang, X., 2017. International Reference Ionosphere 2016: From ionospheric climate to real-time weather predictions. Space Weather 15, 418–429. https://doi.org/10.1002/2016SW001593.

Bjoland, L.M., Belyey, V., Løvhaug, U.P., La Hoz, C., 2016. An evaluation of International Reference Ionosphere electron density in the polar cap and cusp using EISCAT Svalbard radar measurements. Ann. Geophys. 34, 751–758. https://doi.org/10.5194/angeo-34-751-2016.

Friedrich, M., Pock, C., Torkar, K., 2018. FIRI-2018, an updated empirical model of the lower ionosphere. J. Geophys. Res.: Space. Physics 123, 6737–6751. https://doi.org/10.1029/2018JA025437.

Gillies, R. G., van Eyken, A., Spanswick, E., Nicolls, M. J., Kelly, J., Greffen, M., Knudsen, D., Connors, M., Schultzer, M., Valentic, T., Malone, M., Buoncore, J., St-Maurice, J.-P., Donovan, E., 2016. First observations from the RISR-C incoherent scatter radar. Radio Sci., 51, 1645-1659. https://doi.org /10.1002/2016RS006062.

Greenwald, R.A., Frissell, N.A., de Larquier, S., 2016. Using ray tracing to evaluate the performance of several methods for determining the ground range and refractive index of ionospheric scattering volumes. AGU Fall Meeting Abstracts.

Greenwald, R.A., Frissell, N., de Larquier, S., 2017. The importance of elevation angle measurements in HF radar investigations of the ionosphere. Radio Sci. 52, 305–320. https://doi.org/10.1002/2016RS006186.

Koustov, A.V., Ullrich, S., Ponomarenko, P.V., Gillies, R.G., Nishitani, N., 2020. Comparison of SuperDARN peak electron density estimates based on elevation angle measurements to ionosonde and incoherent scatter radar measurements. Earth, Planets and Space 72, 43. https://doi.org/10.1186/s40623-020-01170-w.

Kutiev, I., Tsagouri, I., Perrone, L., Pancheva, D., Mukhtarov, P., Mikhailov, A., Lastovicka, J., Jakowski, N., Buresova, D., Blanch, E., Andonov, B., Altadill, D., Magdaleno, S., Parisi, M., Torta, J.M., 2013. Solar activity impact on the Earth's upper atmosphere. J. Space Weather and Space Climate 3, A06. https://doi.org/10.1051/SWSC/2013028.

Larson, B., Koustov, A. V., Kouznetsov, A. F., Lomidze, L., Gillies, R. G., Reimer, A. S., 2021. A comparison of the topside electron density measured by the Swarm satellites and incoherent scatter radars over Resolute Bay, Canada. Radio Sci., 56, e2021RS007326. https://doi.org/10.1029/2021RS007326.

Lomidze, L., Knudsen, D.J., Burchill, J., Kouznetsov, A., Buchert, S.C., 2018. Calibration and validation of Swarm plasma densities and electron temperatures using ground-based radars and satellite radio occultation measurements. Radio Science 53, 15–36. https://doi.org/10.1002/2017RS006415.

Maltseva, O.A., Nikitenko, T.V., 2021. Validation of various ionospheric models in the high-latitudinal zone. Adv. Space Res. 68 (5), 2233–2243. https://doi.org/10.1016/j.asr.2020.09.016.

Nishitani, N., Ruohoniemi, J.M., Lester, M., Baker, J.B.H., Koustov, A. V., Shepherd, S.G., Chisham, G., Hori, T., Thomas, E.G., Makarevich, R.A., Marchaudon, A., Ponomarenko, P., Wild, J., Milan, S., Bristow, W.A., Devlin, J., Miller, E., Greenwald, R.A., Ogawa, T., Kikuchi, T., 2019. Review of the accomplishments of mid-latitude SuperDARN HF radars. Progress in Earth and Planetary Science 6 (1), 1–57. https://doi.org/10.1186/s40645-019-0270-5.

Ponomarenko, P.V., St-Maurice, J.-P., Waters, C.L., Gillies, R.G., Koustov, A.V., 2009. Refractive index effects on formation and velocity estimates of ionospheric HF backscatter echoes. Ann. Geophys. 27, 4207–4219. https://doi.org/10.5194/angeo-27-4207-2009.

Rawer, K., 2013. Wave propagation in the ionosphere, Developments in electromagnetic theory and applications, Springer Science and Business Media.

Shaikh, M.M., 2022. On the use of empirical models for high-latitude ionosphere. J. Atmos. Solar-Terr. Phys. 238–23. https://doi.org/10.1016/j.jastp.2022.105935.

Shubin, V.N., 2015. Global median model of the F2-layer peak height based on ionospheric radio-occultation and ground-based Digisonde observations. Adv. Space Res. 56, 916–928. https://doi.org/10.1016/j.asr.2015.05.029.

Themens, D. R., Jayachandran, P. T., McCaffrey, A. M., 2019b. Validating the performance of the Empirical Canadian High Arctic Ionospheric Model (E-CHAIM) with in situ observations from DMSP and CHAMP. J. Space Weather and Space Climate 9, A2. https://doi.org/10.1051/swsc/2019021.

Themens, D. R., Jayachandran, P. T., Reid, B., McCaffrey, A. M., 2020. The limits of empirical electron density modeling: Examining the capacity of E-CHAIM and the IRI for modeling intermediate (1- to 30-day) timescales at high latitudes. Radio Sci., 54. https://doi.org/10.1029/2018RS006763.

Themens, D. R., Reid, B., Jayachandran, P. T., Larson, B., Koustov, A. V., Elvidge, S., McCaffrey, A. M., Watson, C., 2021. E-CHAIM as a model of total electron content: Performance and diagnostics. Space Weather, *19,* e2021SW002872. https://doi.org/10.1029/2021SW002872.

Themens, D.R., Jayachandran, P.T., Galkin, I., Hall, C., 2017. The Empirical Canadian High Arctic Ionospheric Model (E-CHAIM): N_mF_2 and h_mF_2. J. Geophys. Res.: Space Phys. 122, 9015–9031. https://doi.org/10.1002/2017JA024398.

Themens, D.R., Jayachandran, P.T., Bilitza, D., Erickson, P.J., Häggström, I., Lyashenko, M.V., Reid, B., Varney, R.H., Pustovalova, L., 2018. Topside electron density representations for middle and high latitudes: A topside parameterization for E-CHAIM based on the NeQuick. J. Geophys. Res.: Space Phys. 123, 1603–1617. https://doi.org/10.1002/2017JA024817.

Themens, D.R., Jayachandran, P.T., McCaffrey, A.M., Reid, B., Varney, R.H., 2019a. A bottomside parameterization for the Empirical Canadian High Arctic Ionospheric Model (E-CHAIM). Radio Sci. 54, 397–414. https://doi.org/10.1029/2018RS006748.

Watson, C., Themens, D. R., Jayachandran, P. T., 2021. Development and validation of precipitation enhanced densities for the Empirical Canadian High Arctic Ionospheric Model. Space Weather, 19, e2021SW002779. https://doi.org/10.1029/2021SW002779.